Technical Report
RAL-TR-2006-004

CCLRC

The Imaging Performance of an Argon-Filled Gas Microstrip Detector with Pixellated Readout - A Monte - Carlo Model

J.E.Bateman

May 2006

Council for the Central Laboratory of the Research Councils

RAL-TR-2006-004

THE IMAGING PERFORMANCE OF AN ARGON-FILLED GAS MICROSTRIP DETECTOR WITH PIXELLATED READOUT - A MONTE-CARLO MODEL

J. E. Bateman

Rutherford Appleton Laboratory, Chilton, Didcot, Oxon, OX11 0QX, UK

4 April 2006

Abstract

A previously developed Monte-Carlo model is used in a computer study to examine the expected imaging performance of the type of one-dimensional x-ray imaging detector being developed for application on the new Synchrotron Radiation Source (DIAMOND) at Rutherford Appleton Laboratory.

1. Introduction

The imaging gas avalanche counter is a long-established option for x-ray imaging in the energy range of a few to around 20keV, for a wide range of applications in bio-medical, materials science and astronomy. At Rutherford Appleton Laboratory (RAL) recent efforts have been concentrated on the development of the gas microstrip detector (GMSD) [1] as a high rate, high spatial resolution detector for x-ray scattering experiments on Synchrotron Radiation Sources (SRS) and neutron scattering experiments on Spallation Neutron Sources (SNS). This work is based on the extensive work by many groups (world-wide) to make the GMSD a possible technology for application in the extreme conditions of particle tracking in Particle Physics [2]. Examples of this are seen in references [3,4] and on-going developments of these technologies are well advanced for application on the new RAL SRS machine (DIAMOND) currently under construction and the existing SNS machine (ISIS). In the course of these developments it was found that computer modelling could materially assist the design and prototyping stages of the projects [5].

The spatial resolution obtainable from an x-ray gas avalanche counter results from a convolution of the basic physical conversion and amplification processes with the precise treatment which the readout applies to determine a spatial resolution parameter. The first stage of this process is essentially quantised and stochastic in nature and so eminently suitable for simulation in a Monte-Carlo model. In the context of the development of the GMSD a key interest is in the interaction of the conversion "resolution" with the sampling limitations of the detector strip widths. This is the work presented in this report.

2. Spatial Resolution of X-rays in Gas Avalanche Detectors

Practical exploitation of x-ray gas imaging counters is conventionally centred on the copper K_α line energy at 8keV although applications may extend from a few up to ≈20keV. In this range the noble gas argon is usually used as the main x-ray converter combined with a fraction of quencher gas – typically 10% to 20% of a suitable hydrocarbon. The quencher has essentially negligible x-ray stopping power but is essential for stabilising the avalanche process and cooling the secondary electrons in their drift to the amplifying anode.

The primary interaction of an x-ray with a (noble) gas atom is usually to eject a photo-electron from an accessible atomic shell (K,L,M in the case of argon) leaving behind a primary hole which is filled either by a fluorescent process (in which a lower energy x-ray is emitted) or by an auger electron (again of lower energy). These in turn leave a hole in a lower shell which is filled from even lower energy shells with a cascade of very low energy electrons which dissipate the residual energy of the event. The photo-electrons (PE) and auger electrons (AE) ionise the counter gas locally to the x-ray interaction and the secondary electrons then drift down under the influence of a suitable drift field towards the high electric field of the amplifying anodes. There in the high electric field each secondary electron generates its own avalanche (usually aggregated by the amplifier time constants used in the readout system) to generate a

plasma of electrons and ions which is separated by the electric field to generate the dipole signal which is detected by the readout amplifiers.

In our x-ray energy range the dominant (K-shell) fluorescent yield in argon is ≈10%. The argon K fluorescence (≈3keV) has an attenuation length of 3.18cm in pure argon and generally escapes from a detector of typical centimetre dimensions without converting. In other words the useful spatial resolution of the gas detector originates in the PE/AE energy deposits only.

The readout amplifiers can be attached either to the anode electrodes or (for example) to mutually orthogonal strips on cathode planes which detect the dipole induction signal released as the positive ion cloud leaves the anode region. There are various readout methods which develop a spatial position parameter from these pulses – resistive divide [6], coupling cathode induction pulses to artificial delay lines [7], using differential induction pulse pick-up [8], putting analogue to digital converters (ADC) on either anode or cathode strips and evaluating the centroid of the distribution [9], or finally, one can with fine amplifying structures, rely on the spatial position of the structure and simply count the pulses in each channel [10]. In the present report one is concerned with predicting the spatial resolution and readout efficiency of the Wide Angle Scattering detector (WAXS) under development for DIAMOND which uses a pixellated readout (i.e. the last option enumerated above). The details of the Monte-Carlo modelling software used has been described in detail elsewhere [11] and only minor modifications are required to simulate the simple channel by channel (i.e. pixellated) readout system employed in this case.

3. The Model Detector Specifications

The simulation software can deal with any desired detector dimensions. For the purposes of this study a GMSD with "pointing" anodes is assumed with an active drift depth of 25mm and a maximum anode pitch of 500μm. (In a "pointing" design [12,3] the x-rays enter the active volume parallel to the GMSD anodes which point at the scattering sample so that the conversion efficiency can be maximised and the rate density on the anode minimised while keeping the drift distances of the secondary electrons minimised.) However, the results are used more generally to examine the effects of strip width. Each strip is equipped with its own charge and shaping amplifier which feeds a discriminator and scaler dedicated to that strip. This approach offers the possibility of counting at very high rates in every channel without the significant dead times associated with interpolating readouts. The counting threshold (LLD) on each channel is independently controlled and is the only electronic set-up parameter required. As will be shown, the LLD controls both the spatial resolution and the readout efficiency of the detector. In the simulations only the readout efficiency is evaluated: this is the fraction of converted x-rays which are accepted by the data capture system. The overall detection efficiency is the product of this fraction with the conversion efficiency, which is controlled by the nature, pressure and dimensions of the active gas volume.
The other parameters maintained constant are as follows: gas avalanche gain = 1000, amplifier noise = 3000 electrons RMS (root mean square) and a diffusion constant (dependent on the gas mixture and drift field) of σ_0=200μm/√cm. Events are generated uniformly over the conversion depth in the simulations. The stochastic

noise generated in the charge signal by the conversion, avalanche and electronic amplification processes are integrated into the model.

4. The Simulations

4.1 The Event Footprint

As noted in the previous report [11], the secondary electron (SE) charge cloud which gives rise to the signal in the detector is subject to spreading principally from diffusion during the drift towards the anode and the effects of the photo/auger electron (PE/AE) range of the primary fast electrons. Averaging over a large number of x-ray events ($\approx 10^3$) gives a smooth distribution of the (average) hit pattern across the GMSD anode plane. This may be referred to as the footprint of events of a given x-ray energy. This footprint gives a clear indication of the behaviour of the spatial resolution whether an interpolating readout or a pixellated readout is used.

Figure 1 shows a set of footprint curves for x-ray energies (E_x) between 2keV and 10keV and figure 2 expands the energy range up to 20keV. The strip width is set artificially low at 100μm to eliminate sampling errors from the curves. In the low energy range, the curves are close to normal distributions showing the dominance of the diffusion process, while towards E_x=20keV the long tails show the dominance of the PE range. Figure 3 summarises the data of figures 1 and 2 by plotting the full width at half maximum (FWHM) and full width at one tenth maximum (FWTM) of the footprints as a function of E_x. The FWHM curve shows the characteristic optimum in argon at about $E_x \approx 5$keV seen previously in the optimisation studies [11] but it is clear that counting above a simple threshold as in the case of the pixellated readout will not give spatial resolution much better than 500μm (FWHM) at the standard x-ray energy of 8keV.

It will be noted that figures 1 and 2 (being averages) do NOT show the strong variability found in the footprint of individual events. This is dominated by the stochastic noise from the small number (a few hundred) of secondary electrons and the random dispersion caused by the drift diffusion and the primary electron ranges.

4.2 Spatial Resolution

The readout method in the present study is simply to count triggers accepted above the discriminator level (LLD) in the scaler attached to each strip. In the practical case of relatively wide (0.5mm, say) strips, the spatial sampling of an incident line source is inevitably crude in terms of the footprints displayed above. (Figure 4 shows a typical example.) Thus some care is required in selecting a statistic to represent the effective spatial resolution of the detector. The fitting of a normal curve to the hit pattern is a valid option; but time consuming. Calculating the standard deviation (SD) of the hit pattern (in bins) and adding it in quadrature to the geometric SD of a bin ($1/\sqrt{12}$) gives essentially the same result as the fitting process as figure 4 illustrates. The FWHM (taken as 2.36 x SD) is used as the spatial resolution parameter throughout the studies.

As described in ref. [11] an incident line is modelled as being distributed uniformly over the width of a strip in order to produce a true spatially averaged response. Figure 5 shows a typical spatial response curve of the detector model over the X-ray energy range of 2 – 20keV with the detector specifications listed on the figure. With strips of 500μm the FWHM is relatively constant at ≈750μm for X-ray energies up to E_x=8keV, determined chiefly by the effect of electron diffusion on the footprint. Above this energy the effects of the photo-electron range becomes significant.

As seen in the basic studies with the model [11] the spatial resolution is not found to be very sensitive to the electronic noise (around the typical values experienced in practice) and is only weakly sensitive to the conversion depth (again around practical values of a few centimetres). The only electronic "set-up" parameter is the LLD and, as figure 6 shows, this has a significant effect on the FWHM at E_x=8keV, almost halving it as the LLD increases from $0.3E_{xp}$ to $0.7E_{xp}$. (E_{xp} is the mean pulse height produced at the discriminator by the detection of the whole incident X-ray energy, E_x.) Figure 7 shows the improved spatial resolution relative to that seen in figure 5 over the whole energy range when the LLD is increased from $0.3E_{xp}$ to $0.5E_{xp}$. However, the improvement is obtained at some cost of readout efficiency.

4.3 Readout Efficiency

Concealed beneath the average footprints of figures 1 and 2 is the fact of there being two extremal types of individual events: those in which most of the secondary electron signal is collected by one strip and those in which the signal is spread more evenly over at least two strips. With a low LLD setting both types will register in the appropriate scalers with the latter type typically registering two (adjacent) counts. Contrariwise, with a high LLD setting the spread events may be missed entirely. This effect results in two important properties of this type of readout: (a) the readout efficiency decreases quite rapidly as the LLD increases and (b) the overall system occasionally counts a single X-ray more than once at low LLD values. The model therefore records two readout efficiency values: the *apparent readout efficiency,* which is the sum of all counts recorded divided by the number of interacting X-rays and the *readout efficiency*, which is the number of hit patterns recorded divided by the number of incident X-rays. The latter parameter is the figure which determines the statistical value of the data. Figure 6 shows the typical behaviour of these two parameters as a function of LLD under the conditions specified on the figure – though this behaviour is in fact general with the readout efficiency declining (along with the FWHM) as the LLD is increased. Around an LLD value of $0.5E_{xp}$ the apparent readout rate tends to the true readout rate and the normalisation of the X-ray counts is preserved. Thus, LLD selection presents an optional trade-off between spatial resolution and readout efficiency.

How this plays out as a function of energy is exhibited in figure 7 where an LLD of $0.5E_{xp}$ is selected. The optimal spatial resolution (i.e. the FWHM at E_x≈6keV) is approximately the strip width (500μm) and the readout efficiency is just under 80%. The spatial resolution is prevented from rising dramatically with the X-ray energy (above 10keV) because the LLD selects the core of the footprints seen in figure 2. However, a severe cost is paid in the shape of a declining readout efficiency, which is

(of course) compounded with a rapidly falling conversion efficiency in this energy range.

4.4 Readout Uniformity

It is a general aim in the design of a digital imaging detector to achieve a uniformity between channels (differential non-linearity) of a few percent. Variations in counter gain and component tolerances in the amplifier chain leading up to the discriminator make it difficult to reduce the intrinsic variation below ≈5% (RMS or SD). The steep slope in the plot of the apparent efficiency against the LLD setting in figure 6 warns us that this intrinsic spread will be amplified by the interaction of the readout with the signal footprints of figures 1 and 2. The effect is quantified by a parameter called the differential non-linearity multiplier (DNM) which is characterised as follows. In figure 6 let us denote the apparent readout efficiency by the symbol y and the corresponding LLD setting by x. Then DNM = $(dy/y) / (dx/x) = (x/y)\ (dy/dx)$ where the final term is just the gradient of curve in figure 6. For most of the range of LLD (x) this curve is approximately linear (i.e. dy/dx is constant ≈3.2) and evaluating the expression at LLD = 0.5 (a typical setting) gives DNM = (0.5/0.79) 3.2 = 2.03. In other words the intrinsic manufacturing variation is doubled to ≈10%.

This effect leads to the only serious set-up procedure required with this type of readout, namely the normalisation of the readout channel responses. This is effected by scanning a wide beam across the detector and adjusting the LLD settings (usually by computer control) to bring the counting rates into agreement within the desired limits. A prototype MSGD detector developed at RAL achieved a measured uniformity of 3.2% (RMS) after this procedure [10] and it is believed that a figure of 2% is attainable.

4.5 Strip Width Options

One of the attractive possibilities with GMSDs is the ease with which the strip width can be changed. Work elsewhere [2] showed that operation (albeit with reduced gain) could be obtained with pitches less than 200μm. The model was therefore used to evaluate the effect of reducing the strip width on the spatial resolution. All other parameters were kept as before and the LLD chosen in each case to maintain a readout efficiency of 80% at an X-ray energy of 8keV. The results are shown in figure 8.

The first striking feature of figure 8 is that the FWHM is greater than the intrinsic bin resolution ($2.36*x/\sqrt{12}$ in figure 8), the strip width itself, or the sum of the intrinsic strip resolution and the calculated limiting physical resolution [11] in quadrature. Moreover, the observed FWHM is not a strong function of the strip pitch, increasing from 400μm for a 200 μm strip to 580μm for a 500μm strip. These effects are due to the fact that the footprint for E_x=8keV in figure 1 is fixed in spatial extent and the signal is simply subdivided into statistically poorer samples as the detector pitch is reduced. For the same reason, the DNM deteriorates significantly (figure 8), as does the ratio of the apparent to real readout efficiency (figure 9). Figure 9 shows that the LLD must also be reduced (if a fixed readout efficiency is to be maintained) so reducing the signal to noise ratio in the readout channels.

Added to the results shown in figures 8 and 9, the well-established experience that GMSDs become less stable to operate at pitches below 500μm [13], the conclusion of these simulations is that a strip width of ≈400μm-500μm is probably optimal. As an aside, it is worth noting that the same conclusion applies equally to a xenon-filled detector (with pixellated readout) in the sub 10keV region of X-ray energy since the SE footprint is determined chiefly by diffusion which is no better (and perhaps marginally worse) in xenon mixtures.

4.6 Interpolative Readout

Recently the GMSD prototype described in ref. [3] has been integrated with the interpolative readout system of the RAPID2 [14] and delivered a spatial resolution of 325μm FWHM from a collimating mask of holes 200μm diameter when irradiated by ≈8keVkeV X-rays[15]. It is simple to adapt the Monte-Carlo model to deliver the centroid of the SE footprints seen in figure 2. The main unknown is the precise signal to noise ratio in the readout channels, so a range of electronic noise parameters are examined. Figure 10 shows the predicted FWHM as a function of X-ray energy. At E_x ≈ 8keV the sampling at 500μm degrades the FWHM only very slightly relative to the ideal results obtained with a bin width of 5μm with zero electronic noise. Increasing the noise per channel up to 24000 electrons (RMS) makes very little difference since the FWHM has become dominated by the PE range at this X-ray energy in argon. It has a predicted value of ≈320μm. This agrees well with the observed FWHM in ref. [15] (325μm). However, if one unfolds the 200μm collimator diameter from the measured FWHM of 325μm, the data from ref. [15] gives an estimate of ≈250μm for the measured FWHM of the interpolated detector readout. The apparent disagreement between the model and the experimental results from the presence of 25% of isobutane in the gas mixture (which has twice the stopping power of argon and so limits the PE range) and the uncertainties in the unfolding procedure. As the parameters on fig 10 show, the FWHM was evaluated with the same digital expansion (adcratio = 16) as used in the RAPID2 hardware.

If one compares the model-derived FWHM predicted for the simple pixellated readout at E_x=8keV (at LLD=0.5 giving a readout efficiency of 80%) one observes 560μm (figure 7) for a 500μm strip width and 526μm for a 400μm strip width (figure 8). (In the "pointing" detector used for the tests the strip width varies from 400μm to 500μm.)

An interesting feature of figure 10 is that as the X-ray energy increases to ≈8keV the FWHM becomes dominated by the photoelectron range to such an extent that the benefits of a good signal to noise ratio and of any interpolation procedure are rapidly lost. With a xenon filling [11] the optimum in the FWHM shifts upwards to ≈8keV before the photoelectron range begins to take control, leading to a useful improvement in the spatial resolution at X-ray energies above this value.

5. Discussion

The success of the one-dimensionally imaging gas microstrip detector with pixellated readout as a high rate WAXS detector has been recently demonstrated at the Daresbury Synchrotron Radiation Source in a test of the system currently being produced at RAL for application on the DIAMOND X-ray source. In an exposure to the diffraction pattern from a sample of high-density polyethylene the detector system captured a spectrum containing 32 million events with a maximum channel count of 1.3 million events in the main peak in a one second exposure [16]. Good, distortion-free imaging is thus obtained at very high data capture rates with relatively simple multi-channel electronics which are well adapted to cheap on-chip production. However, the system has limitations and properties of which the designer and user must be aware in order to make the application optimal to their requirements. The Monte-Carlo models described above are intended to permit the exploration of the properties of this type of detector system. The various trade-offs between spatial resolution, readout efficiency and readout uniformity have been explicitly examined above and need no further summary. A few general conclusions are, however, worth noting.

In the case of an argon gas filling and a 2.5cm conversion depth, the optimal spatial sample (strip width in the case of a GMSD) lies between 400μm and 500μm. At the optimal X-ray energy (6keV), the FWHM of a line source is closely equal to the strip width while at 8keV the FWHM is 15% to 20% higher than the strip width due to the influence of the PE range on the SE footprint. Changing the gas to xenon will restore the situation at E_x=8keV (the optimum energy in xenon) but will not make a significant difference below this energy as the SE footprint is determined chiefly by diffusion in this region and diffusion in xenon mixtures is not better than that in argon. At higher X-ray energies (>8keV, when the PE range comes to dominate) xenon will show considerable advantages over argon and the relatively good spatial resolution obtained in the detector (e.g. figure 7) will be achieved without such a severe loss in readout efficiency.

In the basic studies of the model [11] the usefulness of increasing the detector gas pressure was explored. As noted there, imaging in the higher energy range is improved by restriction of the PE range. However, in the low energy range the imaging benefits are limited by the fact that it is difficult to significantly improve the diffusion constant in noble gas mixtures by increasing the pressure, and diffusion is the main contributor to the SE footprint in this region.

The parameters in the Monte-Carlo model used in this work can be specified at will to represent any particular planned detector with either argon or xenon gas filling permitting the exploration of design options in a flexible way.

References

1. A. Oed, Nucl. Instr. and Meth. **A 261** (1988) 351.

2. F. Sauli, Development of gas microstrip chambers for radiation detection and tracking at high rates, CERN/DRDC/94-45 (1995)

3. J.E.Bateman, J.F.Connolly, G.E.Derbyshire, D.M.Duxbury, J.Lipp, R.C.Farrow, W.I.Helsby, R. Mutikainen, I Suni, Nucl. Instr. and Meth. **A477** (2002) 340-346.

4. J.E.Bateman, N.J.Rhodes, R.Stephenson, **A 477** (2002) 365-371.

5. J.E.Bateman, N.J.Rhodes, R. Stephenson, Rutherford Appleton Laboratory Report, RAL-TR-98-024.

6. R.Berliner, D,F.R.Mildner, O.A.Pringle, J.S.King, Nucl. Instr. and Meth. **185** (1981) 481.

7. S.N.Kaplan, L.Kaufman, V.Perez-Mendez, K.Valentine, Nucl. Instr. and Meth. **106** (1976) 397.

8. R.Allemand and G.Thomas, Nucl. Instr. and Meth. **137** (1976) 141.

9. R.A.Lewis, W.I.Helsby, A.O.Jones, C.J.Hall, B.Parker, J.Sheldon, P.Clifford, M.Hillen, I.Sumner, N.S.Fore, R.W.M.Jones, K.M.Roberts, Nucl. Instr. and Meth. **A 392** (1997) 32-41.

10. J.E.Bateman, G.E.Derbyshire, D.M.Duxbury, A.S.Marsh, N.J.Rhodes, E.M.Schooneveld, E.J. Spill, R. Stephenson, Rutherford Appleton Laboratory Report, RAL-TR-2004-027 also IEEE Trans. Nucl. Sci. **52** No.3 (2005) 736-740.

11. J. E. Bateman, Rutherford Appleton Laboratory Report, RAL-TR-2005-010

12. V. Zhukov, F. Udo, O. Marchena, F.G. Hartjes, F.D.van der Berg, W. Bras, E. Vlieg, Nucl. Instr. and Meth. **A 392** (1997) 83.

13. J.E. Bateman, R. Barlow, G.E. Derbyshire, J.A. Mir and R. Stephenson, Rutherford Appleton Laboratory Report, RAL-TR-2001-031 also Nucl. Instr. and Meth. **A 513** (2003) 273-276.

14. Cernik et. al. J. Synch. Rad. **11** Part 2, (2004) 163-170.

15. Kan-Cheung Cheung, William Helsby, Nick Clague, Richard Farrow, Adrian Marsh, Dominic Duxbury, Edward Spill, Richard Stephenson, to be published in Nucl. Instr. and Meth. A.

16. D. Duxbury, Private Communication.

FIGURE CAPTIONS

1. Plots of the average spatial distribution (slit beam) of the amplified secondary electron (SE) reaching the detector plane (footprints) at lower X-ray energies from a conversion space 2.5cm deep. The detector strip is artificially set at 0.1mm for the purposes of display. The essential parameters of the system are listed on the figure.

2. A complete set of SE footprints for the X-ray energy range of 2keV – 20keV in argon. The parameters are as in figure 1.

3. A summary of the spatial spread of the footprints of figures 1 and 2 expressed as the full widths at half and tenth maximum (FWHM, FWTM).

4. A typical "hit" pattern observed in the simulated digital readout from a slit beam. A Normal Curve fit is shown with the FWHM derived from it and from the computed algorithm.

5. A typical data set produced by the Monte-Carlo simulation showing the FWHM and Readout Efficiencies under the parameters specified. In this case the LLD=30% i.e. LLD=$0.3E_{xp}$.

6. The calculated FWHM and Readout Efficiencies at E_x=8keV as a function of the LLD setting.

7. A data set similar to that of figure 5 with same conditions except LLD=50% .

8. The Monte-Carlo model shows how the FWHM and the DNM (differential non-linearity multiplier) vary with the detector strip width if the LLD is adjusted to keep the true readout efficiency held at 80%.

9. This figure completes the results from the runs of figure 8 by showing the ratio of the apparent to true readout efficiency as the strip width is varied with all other conditions being the same.

10. The FWHM resolution predicted by the model for an interpolating (centroiding) readout with a sample pitch of 500μm with various levels of electronic noise. The Physical Optimum curve is derived by setting the sample width to 5μm.

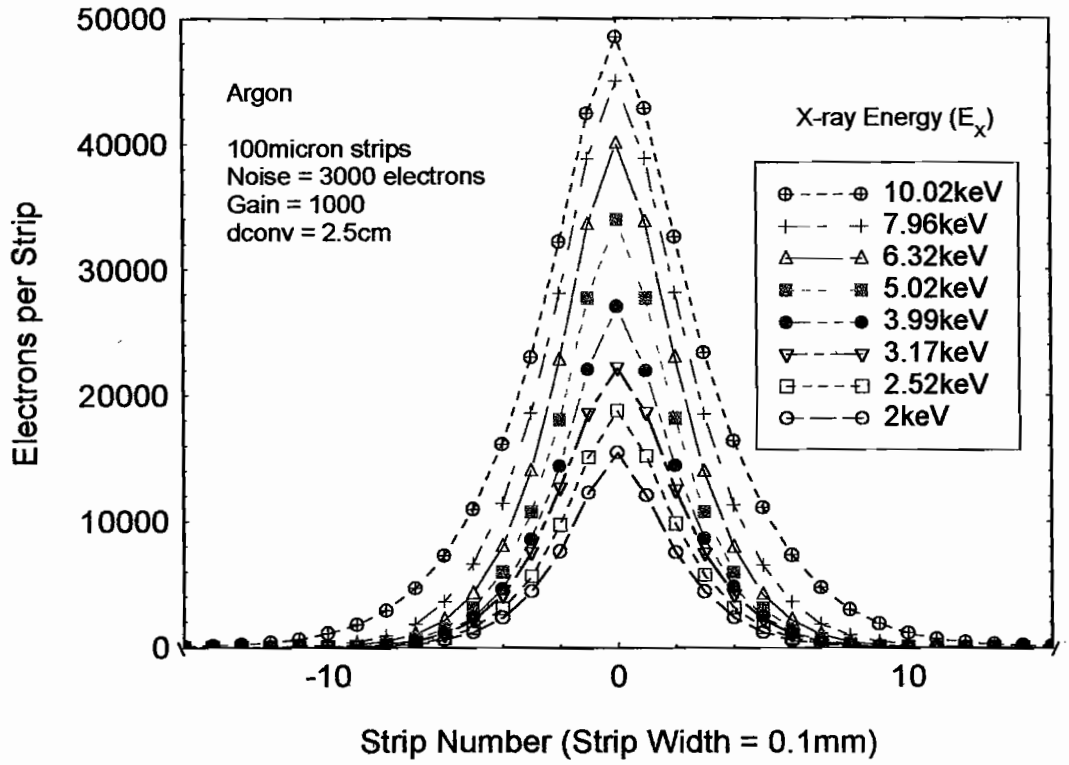

FIGURE 1

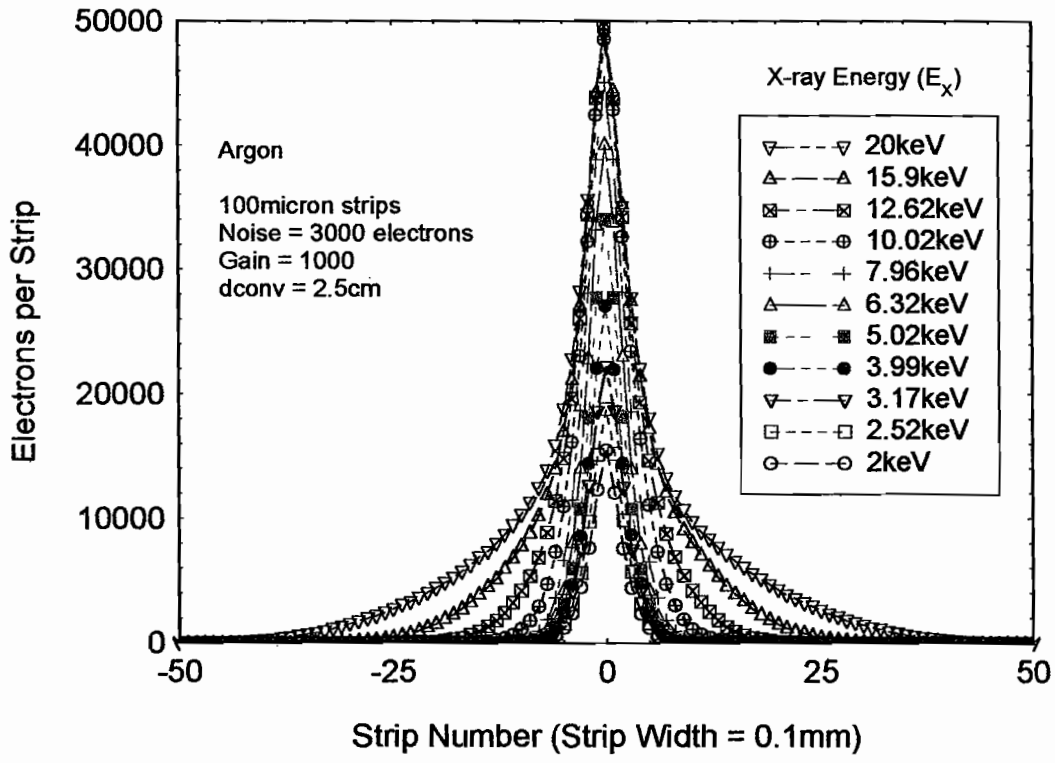

FIGURE 2

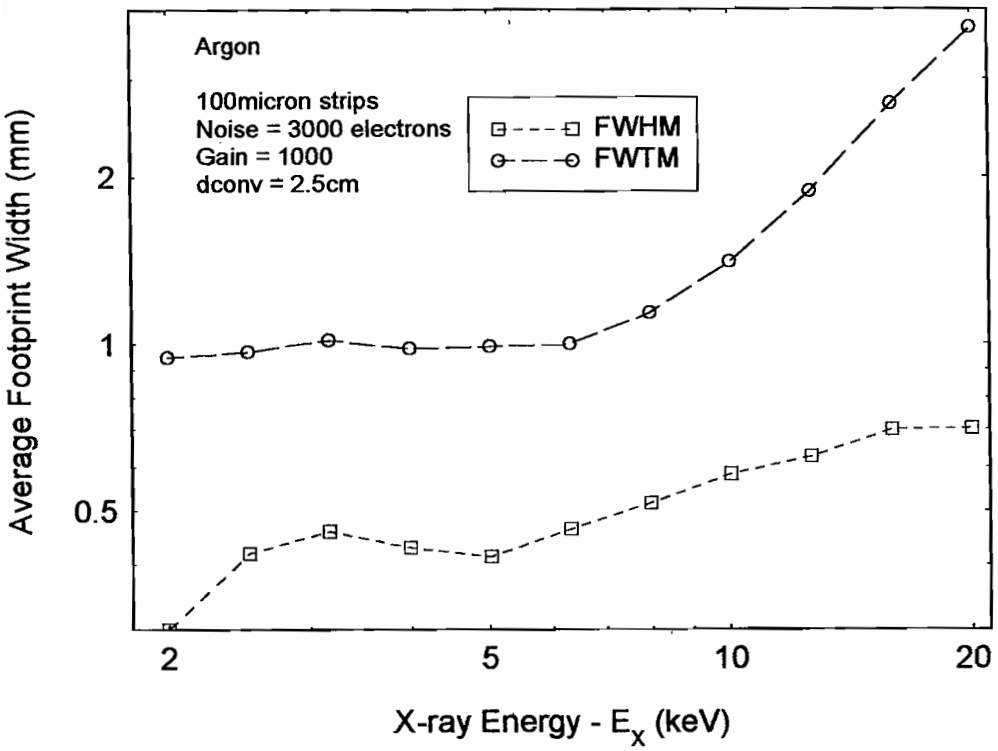

FIGURE 3

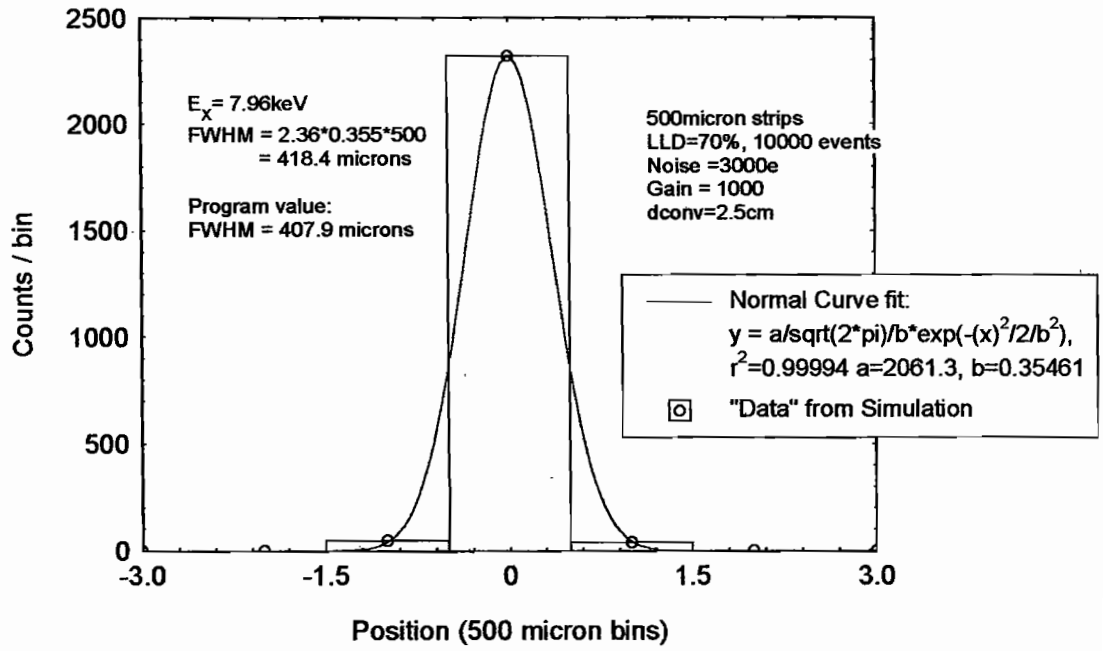

FIGURE 4

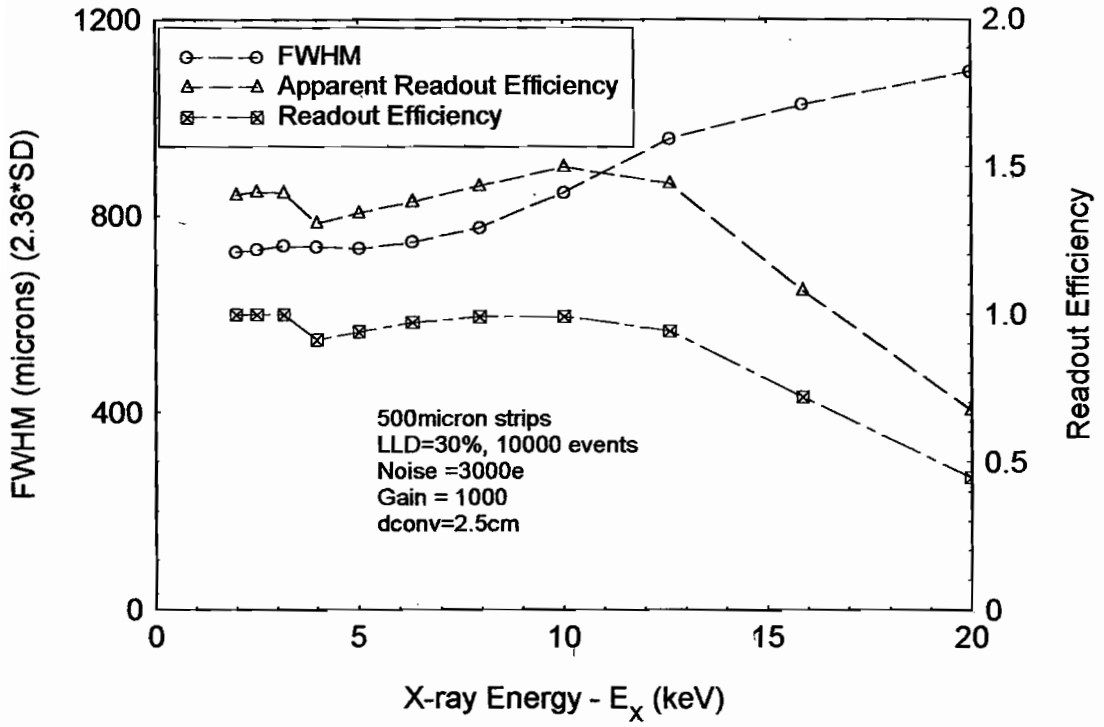

FIGURE 5

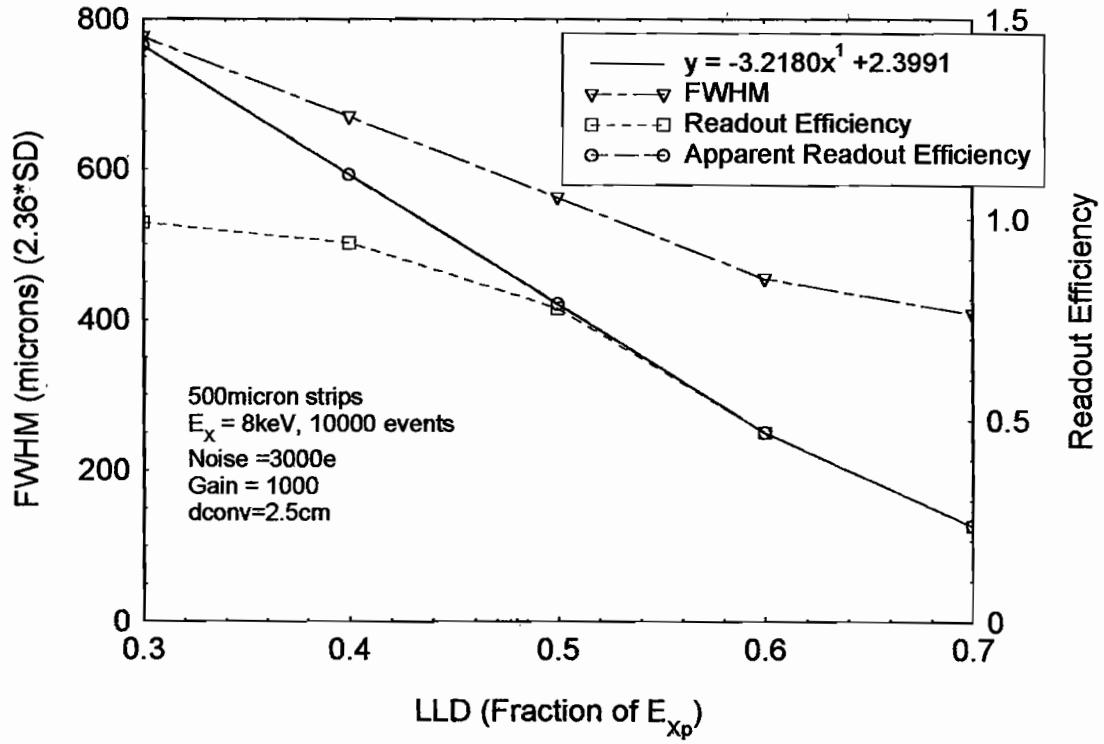

FIGURE 6

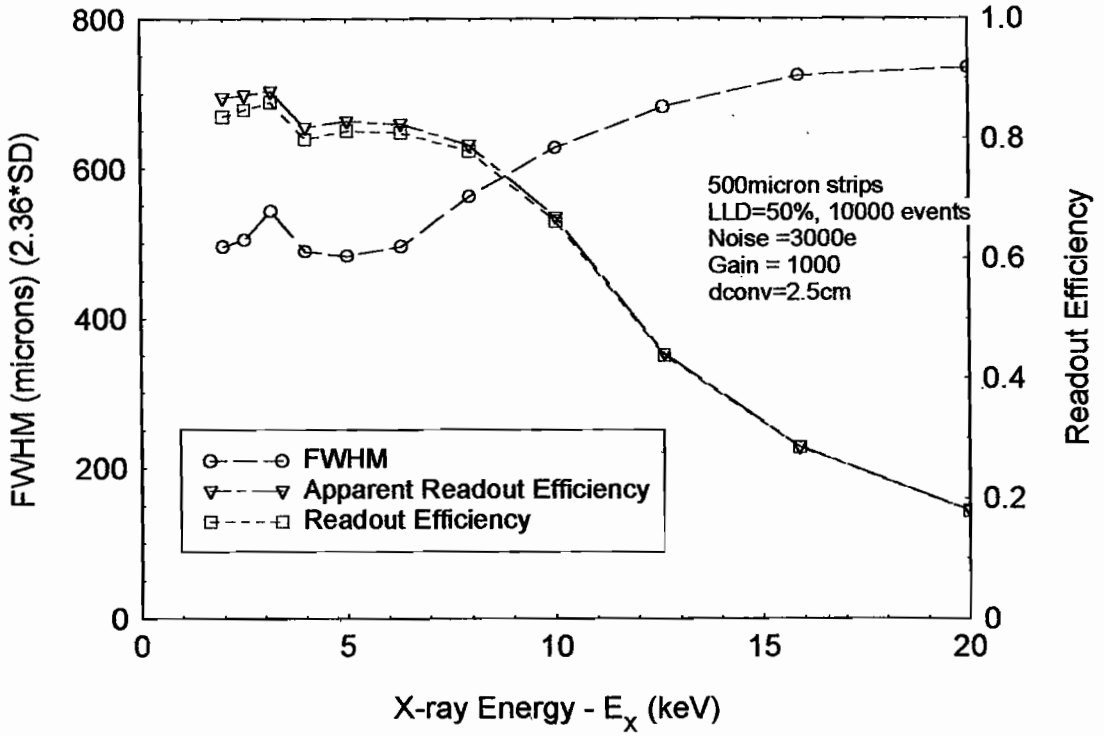

FIGURE 7

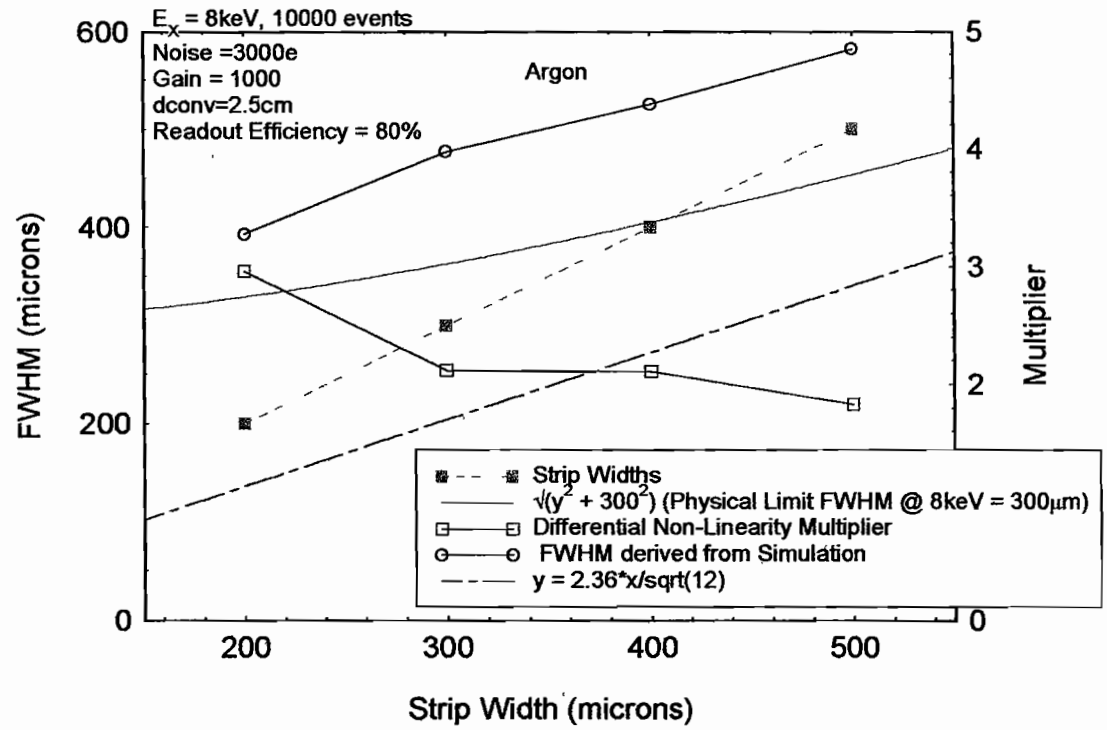

FIGURE 8

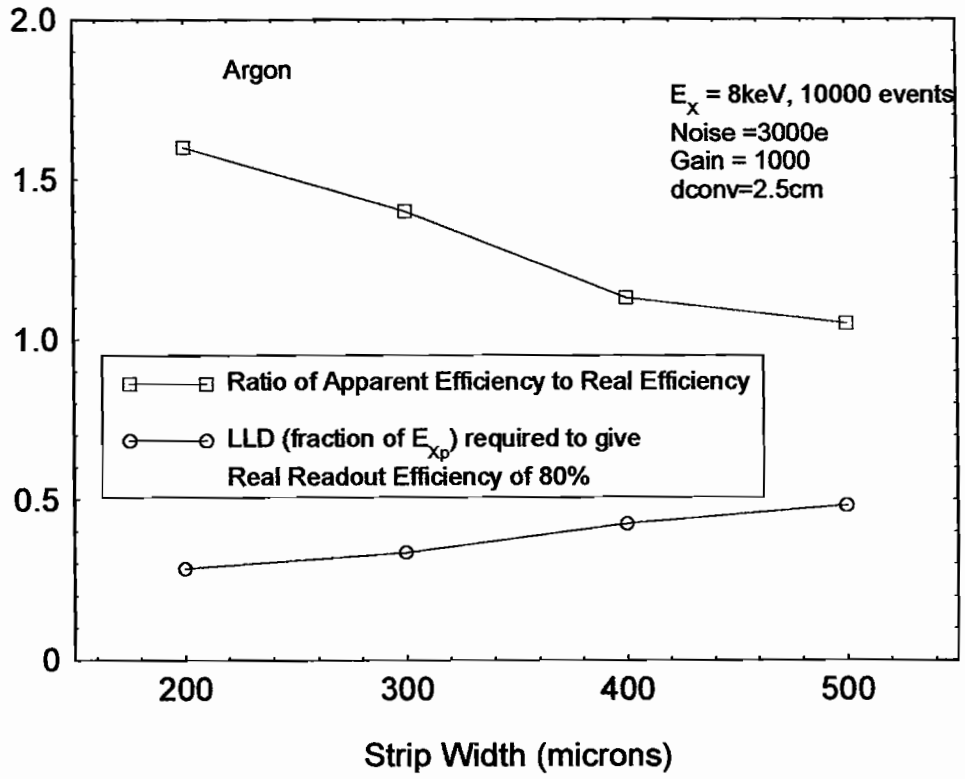

FIGURE 9

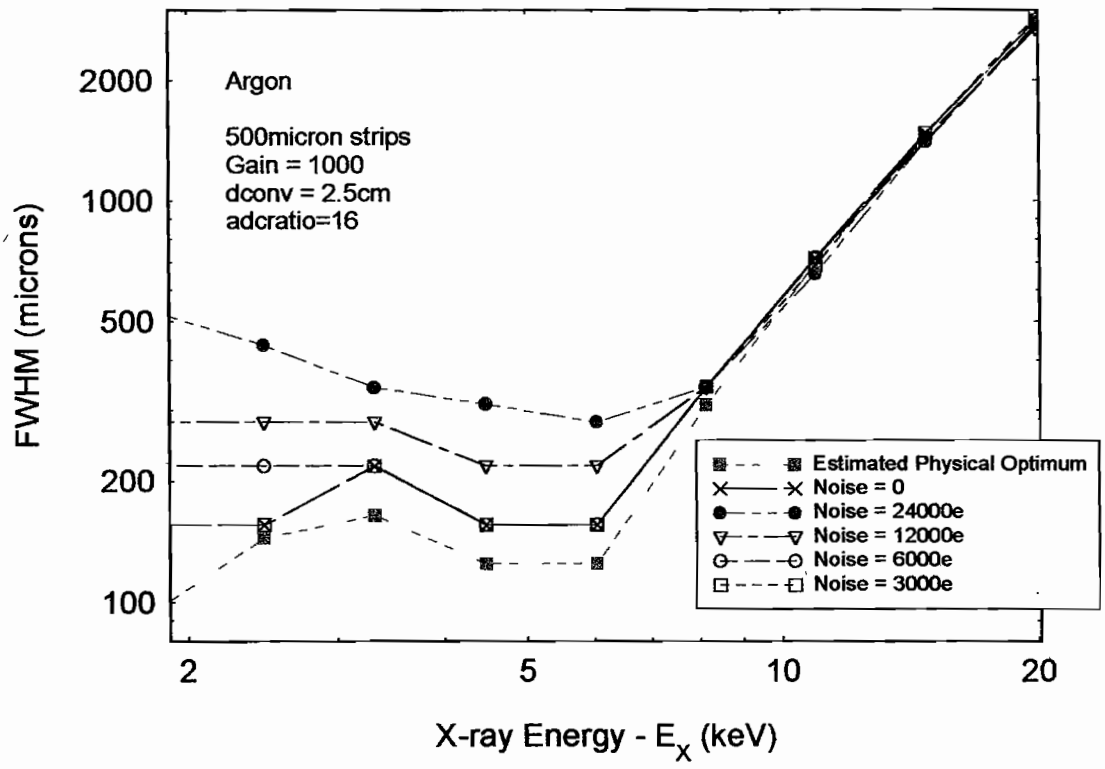

FIGURE 10